Supporting Information

# Remote control of electronic coupling – modification of excited-state electron-transfer rates in Ru(tpy)$_2$-based donor-acceptor systems by remote ligand design

Yusen Luo,[1,2] Jens H. Tran,[1] Maria Wächtler,[1,2] Martin Schulz,[1] Kevin Barthelmes,[3,4] Andreas Winter,[3,4] Sven Rau,[5] Ulrich S. Schubert[3,4] and Benjamin Dietzek*[1,2,4]

[1]*Institute of Physical Chemistry and Abbe Center of Photonics, Friedrich Schiller University Jena, Helmholtzweg 4, 07743 Jena, Germany*

[2]*Department Functional Interfaces, Leibniz Institute of Photonic Technology (IPHT), Albert-Einstein-Straße 9, 07745 Jena, Germany*

[3]*Laboratory of Organic and Macromolecular Chemistry (IOMC), Friedrich Schiller University Jena, Humboldtstraße 10, 07743 Jena, Germany*

[4]*Center for Energy and Environmental Chemistry Jena (CEEC Jena), Friedrich Schiller University Jena, Philosophenweg 7a, 07743 Jena, Germany*

[5]*Institute for Inorganic Chemistry I, Ulm University, Albert-Einstein-Allee 11, 89081 Ulm, Germany*

**Corresponding author: benjamin.dietzek@leibniz-ipht.de*

Experimental details

**UV/Vis Spectroscopy.** The UV/Vis absorption spectra of **D2**-**D4** were recorded with a Cary 5000 UV/Vis spectrometer (Varian, USA) in a 1 cm cuvette at room temperature.

**Time-Resolved Spectroscopy.** Femtosecond (fs) transient absorption (TA) spectra were collected by using a previously reported home-built pump-probe laser system which is based on an amplified Ti: Sapphire oscillator (1 kHz, 800 nm).[1] Samples were excited by pump pulse centered at 520 nm (TOPAS-C, Lightconversion Ltd.) with a duration of 80 fs. The power of the pump beam at the sample position was kept at 0.35 mW with a beam diameter of 112 μm, corresponding to $1.86 \times 10^{20}$ photos $m^{-2}$ per pump pulse. A white light supercontinuum generated by focusing a fraction of the fundamental in a $CaF_2$ plate is used to probe the samples in a wide spectral range (340 to 750 nm). The pump beam is delayed in time with respect to the probe beam by means of an optical delay line and the polarization between probe and pump is set at the magic angle (54.7°). Temperature-dependent fs TA spectra were recorded by putting the sample in a 1 cm cuvette (optical density 0.24 at 520 nm) which was then placed in a temperature-controlled cryostat (Optistat DN, Oxford Instrument) cooled with liquid nitrogen. Temperatures were set by an intelligent temperature controller (ITC 503S, Oxford Instruments) and the real-time temperature inside the cuvette was monitored by a temperature sensor which was connected to a digital multimeter (Keithley 2000 multimeter). Fresh solution was used for the fs TA measurement at each temperature. All samples have been cooled down until stable before starting the pump-probe experiment. The fs TA spectra were displayed after chirp correction. The fs TA data were analyzed by a global multi-exponential fit after exclusion of a temporal window of 500 fs around time-zero in order to avoid contributions of the coherent-artifact region to the data analysis. Furthermore, a spectral band of ca. 20 nm around the pump-wavelength is omitted from the data analysis due to pump-scatter in this spectral range. For all the time-resolved experiments the stability of samples was ensured by recording the UV/Vis absorption spectra (JASCO V-670 spectrometer) at room temperature before and after fs TA measurement.

**Electrochemistry.** Cyclic voltammograms (CVs) of **D2**-**D4** were performed in a three-electrode setup consists of a glassy carbon working electrode, a platinum wire counter electrode and an Ag/AgCl reference electrode. CVs were obtained in dichloromethane with a PC-controlled potentiostat (Zahner Zennium Pro). The scan rate was 200 mV/s which kept consistence with the previous electrochemical measurements for **D1** and **T1**.[2] All potentials given in Table S2 refer to ferrocene as standard.

**Synthesis and Characterization Data. D1**, **T1** and all terpyridine ligands were prepared according to literature procedures.[2] All other chemicals were purchased from commercial suppliers and were used as received. Reactions were monitored by thin-layer chromatography (TLC, silica gel on aluminum sheets with fluorescent marker F254 Merk). $^{1}$H-, $^{13}$C{H}-NMR were recorded at 20 °C on Bruker Advance AC400 and AC600 spectrometers. Chemical shifts are reported in parts per million relative to tetramethysilane ($^{1}$H-, $^{13}$C{H}-NMR), as external standards. The residual signal of the deuterated solvents [d$^{3}$]MeCN, were used as internal standards in $^{1}$H- and $^{13}$C{H}-NMR experiments. J values are given in Hz. ESI-MS mass spectra were recorded either on a Finnigan MAZ95XL or on a Finnigan MAT SSQ 710. The experimental isotope pattern of the respective compound was compared to the calculated isotope pattern. Presented yields are not optimized.

1) General procedure for [Ru(tpy-Ar)]$Cl_3$ complexes

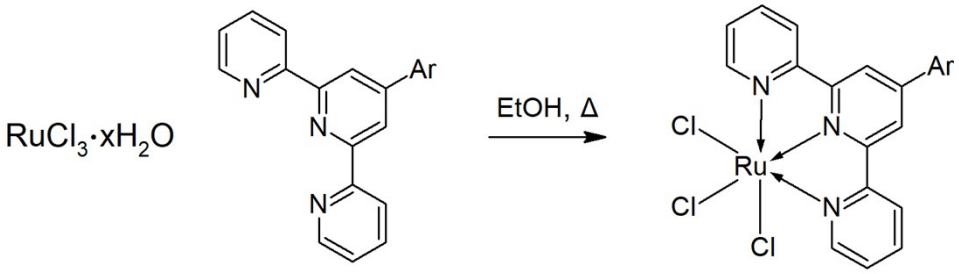


A microwave vial was charged with $RuCl_3$•x$H_2O$ (0.29 mmol), the respective tpy-Ar (0.29 mmol) and EtOH (25 mL). The vial was capped and degassed with nitrogen for 20 min. The suspension was heated to 96 °C for 4h. Subsequently the suspension was filtered and the precipitate was washed with EtOH (30 mL) and diethyl ether (30 mL). After drying *in vacuo* the dark brown crude product was used as received.

**[Ru(tpy-Ph)]$Cl_3$** (124.2 mg, 82%).

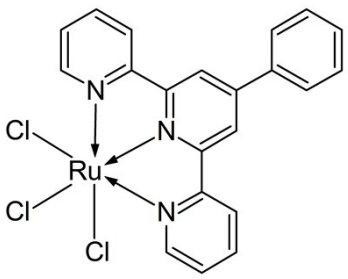

**[Ru(tpy-PhMe)]$Cl_3$** (352.9 mg, 89%)

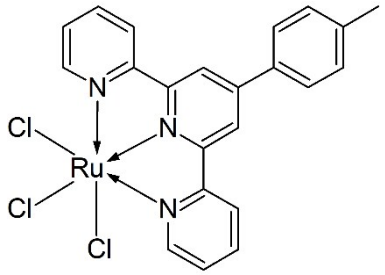

**[Ru(tpy-PhOMe)]$Cl_3$** (217.9 mg, 91%)

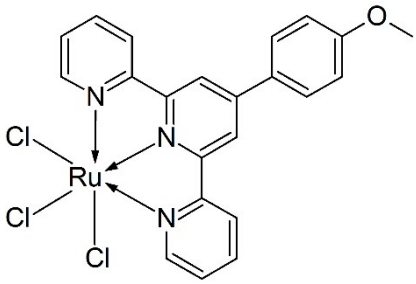

2) General procedure for $[Ru(MeCN)_3(tpy\text{-}Ar)](PF_6)_2$

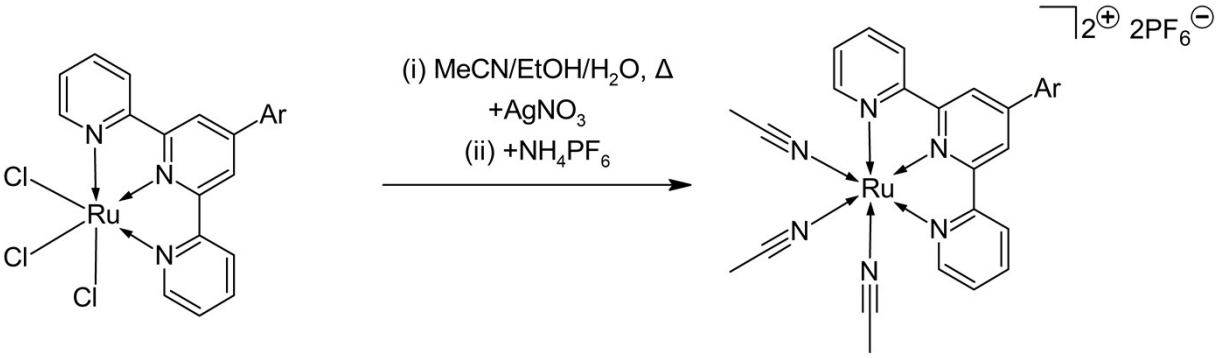


A microwave vial was charged with the respective $[Ru(tpy\text{-}Ar)]Cl_3$ (0.17 mmol) $AgNO_3$ (0.17 mmol) and MeCN/EtOH/water (6:1:1, 18 mL). The vial was capped and degassed with nitrogen for 20 min and heated to 80 °C for 4h. Subsequently the solution was filtered to remove the fine AgCl precipitate. Excess $NH_4PF_6$ was added to the filtrate and the solution was concentrated *in vacuo*. When precipitation occurred water was added and the suspension was centrifuged. The solid was washed with water (2 × 20 mL). The residue was then dissolved in a minimum of MeCN and the product was precipitated in diethyl ether (30 mL). The suspension was centrifuged and the product was obtained as orange/yellow powder and subsequently dried *in vacuo* and used as received.

**[Ru(MeCN)$_3$(tpy-Ph)](PF$_6$)$_2$** (36.6 mg, 26%)

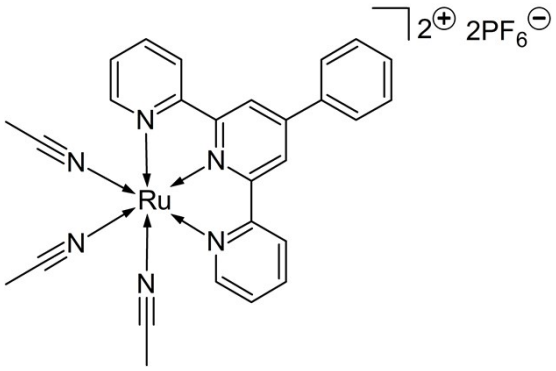


$^1$H NMR (400 MHz, $CD_3CN$): $\delta$ = 8.93 (2H, d, $J$ = 5.3 Hz), 8.65 (2H, s), 8.55 (2H, d, $J$ = 7.9 Hz), 8.21 (2H, td, $J$ = 7.9, 1.5 Hz), 8.01-8.07 (2H, m), 7.73-7.78 (2H, m), 7.66-7.72 (2H, m), 7.64 (1H, d, $J$ = 7.3 Hz), 2.75 ppm (3H, s). $^{13}$C NMR (101 MHz, $CD_3CN$): $\delta$ = 160.0, 159.6, 155.5, 151.0, 140.1, 137.4, 131.7, 130.6, 129.1, 128.8, 125.2, 121.9 ppm.

**[Ru(MeCN)$_3$(tpy-PhMe)](PF$_6$)$_2$** (211.5 mg, 58%)

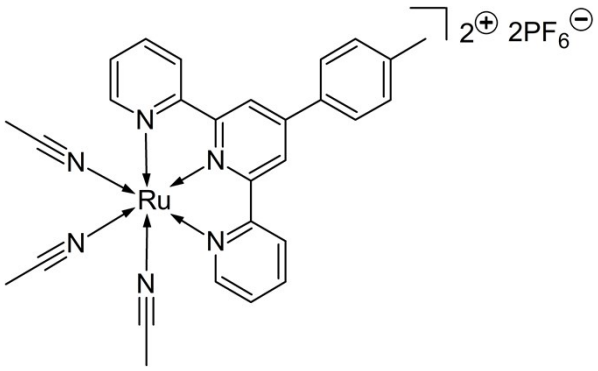


$^1$H NMR (400 MHz, $CD_3CN$): $\delta$ = 8.90-8.96 (2H, m), 8.63 (2H, s), 8.55 (2H, d, $J$ = 7.9 Hz), 8.20 (2H, td, $J$ = 7.9, 1.8 Hz), 7.94 (2H, d, $J$ = 8.5 Hz), 7.75 (2H, ddd, $J$ = 7.7, 5.5, 1.2 Hz), 7.50 (2H, d, $J$ = 7.9 Hz), 2.75 (3H, s), 2.49 ppm (3H, s). $^{13}$C NMR (101 MHz, $CD_3CN$): $\delta$ = 159.9, 159.7, 155.5, 142.4, 140.0, 134.4, 131.4, 131.3, 129.0, 128.6, 125.1, 121.5, 118.4, 118.5, 21.4, 4.3 ppm.

**[Ru(MeCN)$_3$(tpy-PhOMe)](PF$_6$)$_2$** (88.1 mg, 34%)

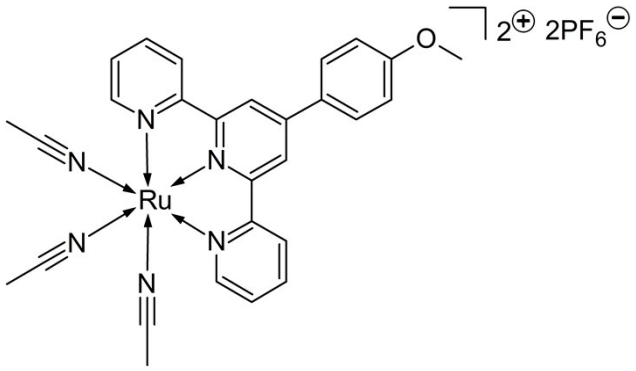

$^1$H NMR (400 MHz, $CD_3CN$): $\delta$ = 8.92 (2Hd, $J$ = 5.0 Hz), 8.61 (2H, s), 8.54 (2H, d, $J$ = 8.2 Hz), 8.20 (2H, td, $J$ = 7.9, 1.5 Hz), 8.03 (2H, d, $J$ = 9.1 Hz), 7.70-7.78 (2H, m), 7.22 (2H, d, $J$ = 8.8 Hz), 3.93 (3H, s), 2.74 ppm (3H, s). $^{13}$C NMR (101 MHz, $CD_3CN$): $\delta$ = 159.8, 159.8, 155.5, 150.6, 143.8, 140.0, 131.0, 130.3, 129.4, 129.0, 125.1, 121.1, 56.4 ppm.

3) General procedure for [Ru(tpy-ptz)(tpy-Ar)](PF$_6$)$_2$ complexes (**D2**-**D4**)

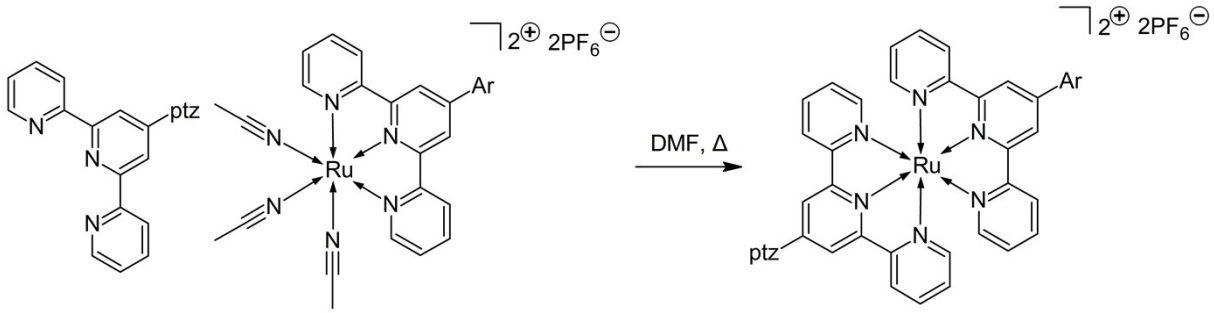

A microwave vial was charge with the respective [Ru(MeCN)$_3$(tpy-Ar)](PF$_6$)$_2$ (0.04 mmol), tpy-ptz (0.04 mmol) and DMF (10 mL). The vial was capped and degassed with nitrogen for 20 min and heated 96 °C for 2-3h. The red crude product was then precipitated in diethyl ether (20 mL) and centrifuged. The red solid was then washed with diethyl ether (5 mL). The crude product was then further purified by column chromatography (silica; MeCN/$H_2O$/satd. aq. $KNO_3$ solution; 40:4:1). An excess of $NH_4PF_6$ was added to the red fraction which was then concentrated *in vacuo*. When precipitation occurred the solution was added to water (30 mL). The formed precipitate was centrifuged and washed with water (2 × 20 mL). After drying *in vacuo* the complex was obtained as dark red powder.

**D2: [Ru(tpy-ptz)(tpy-Ph)](PF$_6$)$_2$** (16.3 mg, 39%)

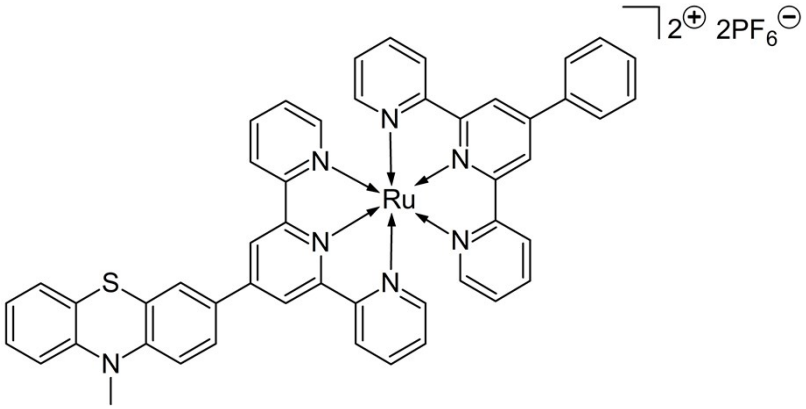


$^1$H NMR (400 MHz, $CD_3CN$): $\delta$ = 9.01 (2H, s), 8.97 (2H, s), 8.64 (4H, d, $J$ = 7.9 Hz), 8.17-8.24 (2H, m), 8.03-8.14 (2H, m), 7.94 (4H, td, $J$ = 7.9, 1.5 Hz), 7.73-7.81 (2H, m), 7.65-7.72 (1H, m), 7.42 (4H, br d, $J$ = 5.6 Hz), 7.28-7.36 (1H, m), 7.22-7.27 (2H, m), 7.13-7.21 (4H, m), 6.99-7.11 (2H, m), 3.52 ppm (3H, s). $^{13}$C NMR (101 MHz, $CD_3CN$): $\delta$ = 159.4, 159.3, 156.6, 156.4, 153.5, 153.5, 149.5, 149.4, 148.9, 148.1, 146.0, 139.1, 138.0, 131.5, 130.7, 129.2, 128.9, 128.5, 128.5, 128.3, 128.1, 126.8, 125.6, 125.6, 125.3, 124.3, 123.1, 122.8, 121.6, 116.2, 116.2, 36.3 ppm. Found C, 50.35; H, 3.01; N, 8.57; S, 2.44. Calc. for $C_{49}H_{35}F_{12}N_7P_2RuS$: C, 51.40; H, 3.08; N, 8.56; S, 2.80. HRMS (Micro-ESI pos) calcd. for $C_{49}H_{35}F_6N_7P^{96}RuS$ [$M^+$] = 994.1402.1549. Found 994.1392.

**D3: [Ru(tpy-ptz)(tpy-PhMe)](PF$_6$)$_2$** (20.0 mg, 14%)

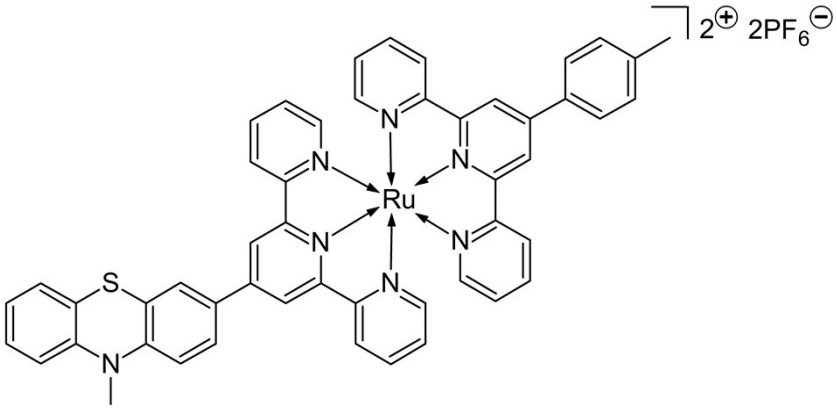


$^1$H NMR (400 MHz, $CD_3CN$): $\delta$ = 8.98 (4H, d, $J$ = 8.5 Hz), 8.64 (4H, d, $J$ = 8.2 Hz), 8.02-8.15 (4H, m), 7.89-7.98 (4H, m), 7.58 (2H, d, $J$ = 8.2 Hz), 7.39-7.47 (4H, m), 7.31 (1H, ddd, $J$ = 8.3, 7.5, 1.5 Hz), 7.22-7.27 (2H, m), 7.17 (4H, ddd, $J$ = 7.3, 5.8, 1.5 Hz), 7.01-7.11 (2H, m), 3.52 (3H, s), 2.54 ppm (3H, s). $^{13}$C NMR (101 MHz, $CD_3CN$): $\delta$ = 159.4, 159.3, 156.5, 156.4, 153.5, 153.5, 149.4, 149.3, 148.9, 148.0, 147.9, 146.0, 142.1, 139.0, 135.0, 131.5, 131.4,

129.2, 128.7, 128.5, 128.4, 128.3, 128.1, 126.8, 125.5, 125.3, 124.3, 123.0, 122.4, 121.6, 116.2, 116.1, 36.3, 21.5 ppm. Found C, 49.33.35; H, 3.36; N, 8.91; S, 2.40. Calc. for $C_{49}H_{35}F_{12}N_7P_2RuS•H_2O•MeCN$: C, 51.28; H, 3.48; N, 9.20; S, 2.63. HRMS (Micro-ESI pos) calcd. for $C_{50}H_{37}F_6N7P^{96}RuS$ [$M^+$] = 1008.1549. Found 1008.1569.

**D4: [Ru(tpy-ptz)(tpy-PhOMe)](PF$_6$)$_2$** (13.0 mg, 11%)

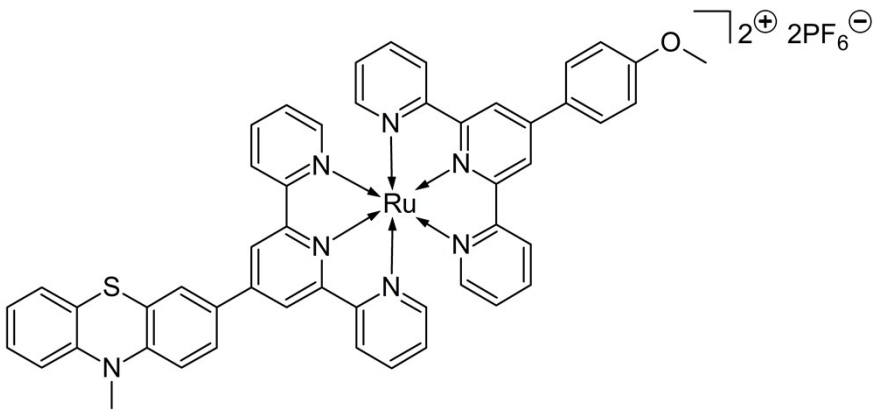


$^1$H NMR (400 MHz, $CD_3CN$): $\delta$ = 9.00 (4H, s), 8.67 (4H, d, $J$ = 8.2 Hz), 8.22 (2H, d, $J$ = 8.8 Hz), 8.06-8.15 (2H, m), 7.96 (4H, t, $J$ = 7.7 Hz), 7.44 (4H, t, $J$ = 5.6 Hz), 7.30-7.37 (3H, m), 7.25-7.30 (2H, m), 7.16-7.23 (4H, m), 7.04-7.12 (2H, m), 4.00 (3H, s), 3.55 ppm (3H, s). $^{13}$C NMR (101 MHz, $CD_3CN$): $\delta$ = 162.8, 159.4, 156.5, 156.4, 156.4, 153.5, 149.0, 149.0, 148.9, 147.9, 146.0, 139.0, 131.5, 130.3, 129.9, 129.2, 128.5, 128.3, 128.1, 126.8, 125.5, 125.3, 124.3, 123.1, 122.0, 121.6, 116.2, 116.1, 116.1, 56.5, 36.3 ppm. HRMS (Micro-ESI pos) calcd. for $C_{50}H_{37}OF_6N_7P^{96}RuS$ [$M^+$] = 1024.1498. Found 1024.1501.

Relaxation scheme of dyads and triad upon excitation at 520 nm

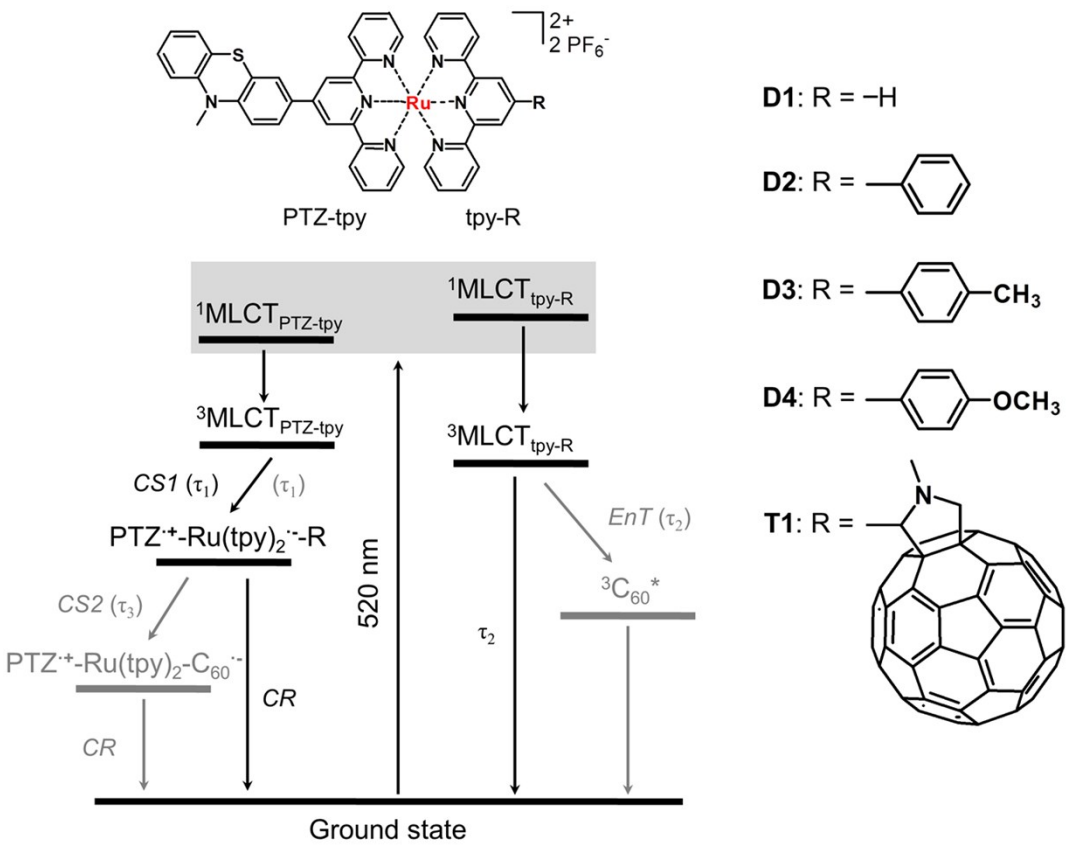


**Figure S1.** Relaxation processes for **D1-D4** and **T1** refer to the model proposed for **D1** and **T1** at room temperature.[3] Terpyridine (tpy) ligand connected with *N*-methylphenothiazine (PTZ) and other substituents are named as PTZ-tpy and tpy-R, respectively. Excitation of $Ru(tpy)_2$ photosensitizer generates two differently distributed MLCT states, *i.e.* $MLCT_{PTZ\text{-}tpy}$ and $MLCT_{tpy\text{-}R}$. The $MLCT_{PTZ\text{-}tpy}$ state decays *via* electron transfer ($\tau_1$, left side) and the $MLCT_{tpy\text{-}R}$ state decays directly to ground state ($\tau_2$, **D1-D4**, right side) or decays *via* energy transfer ($\tau_2$, **T1**, right side, grey lines).

Temperature dependent fs TA data of **D1**

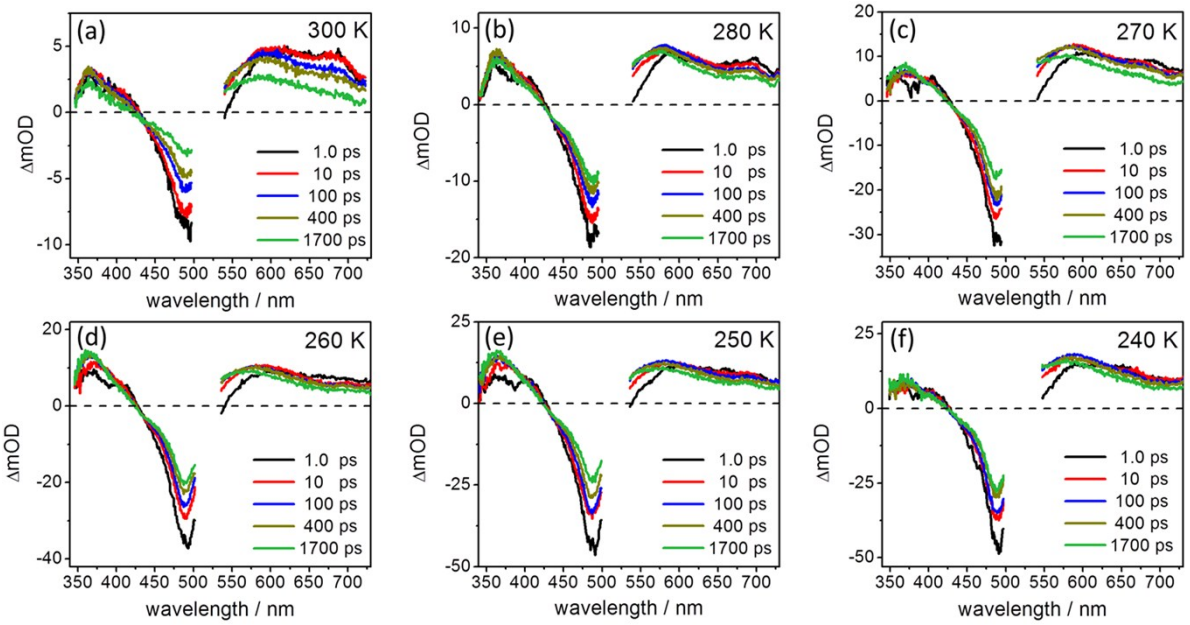


**Figure S2.** fs transient absorption spectra at selected delay times upon excitation at 520 nm in dichloromethane at temperature regions from 300 to 240 K.

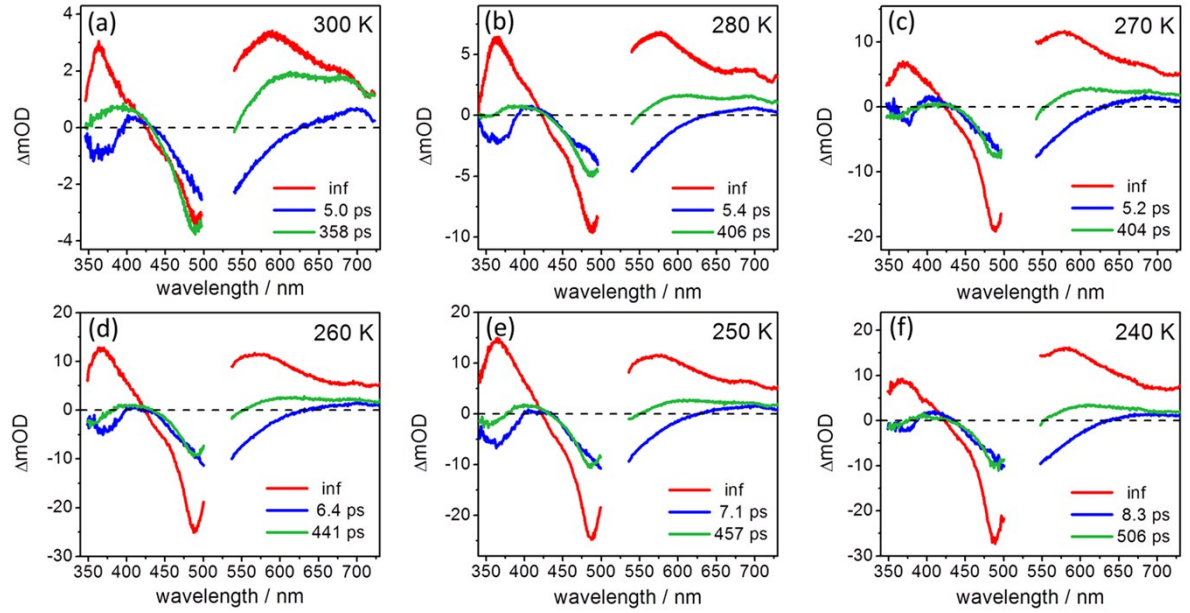


**Figure S3.** Decay-associated spectra resulting from the global fit of fs TA data upon excitation at 520 nm in dichloromethane.

Temperature dependent fs TA data of **D2**

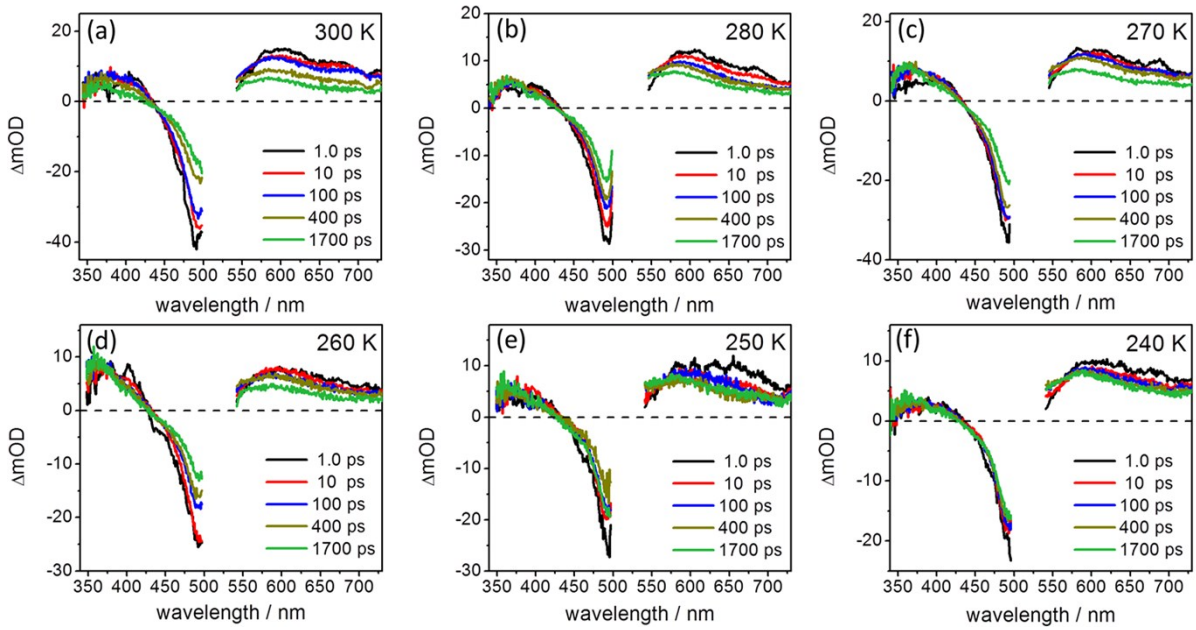


**Figure S4.** fs transient absorption spectra at selected delay times upon excitation at 520 nm in dichloromethane at temperature regions from 300 to 240 K.

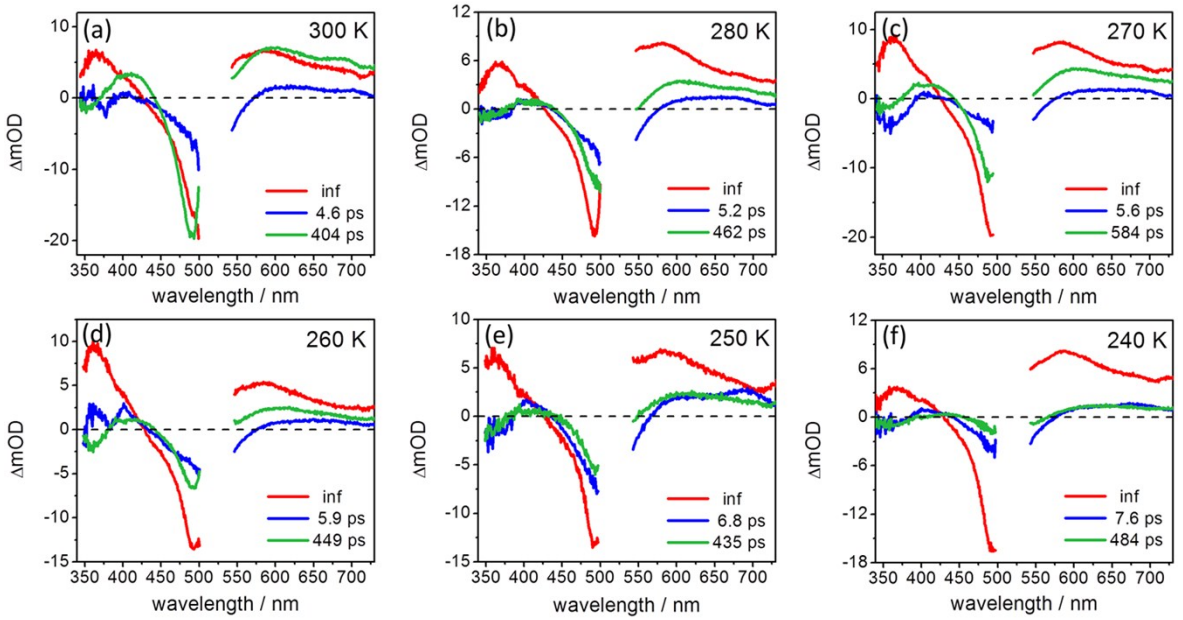


**Figure S5.** Decay-associated spectra resulting from the global fit of fs TA data upon excitation at 520 nm in dichloromethane.

Temperature dependent fs TA data of **D3**

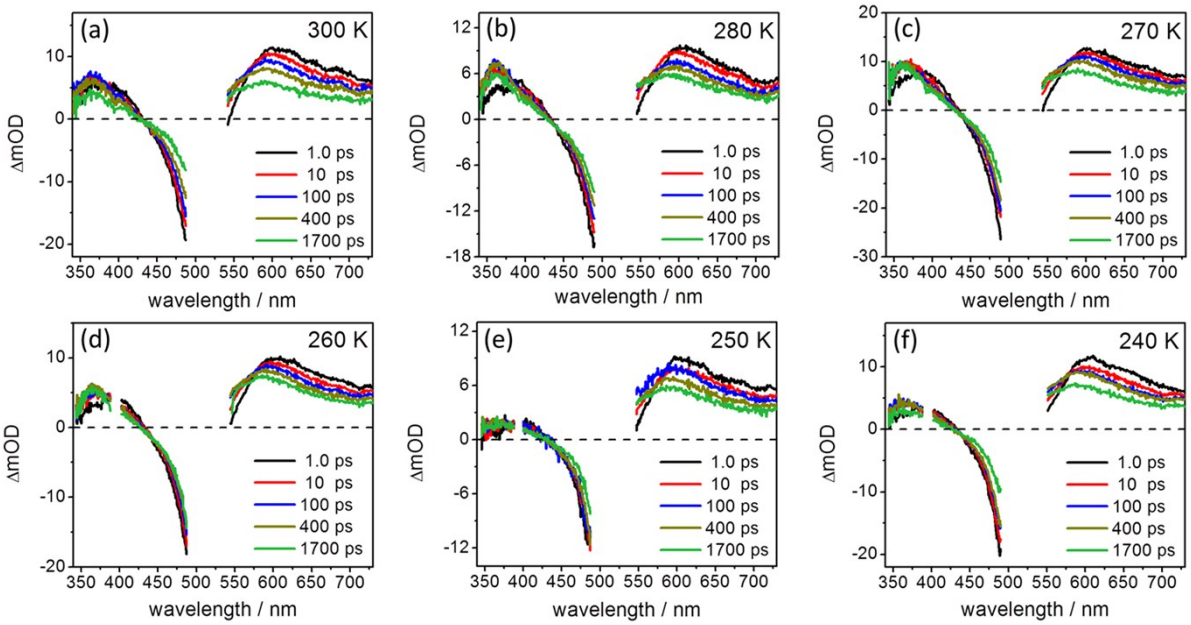


**Figure S6.** fs transient absorption spectra at selected delay times upon excitation at 520 nm in dichloromethane at temperature regions from 300 to 240 K.

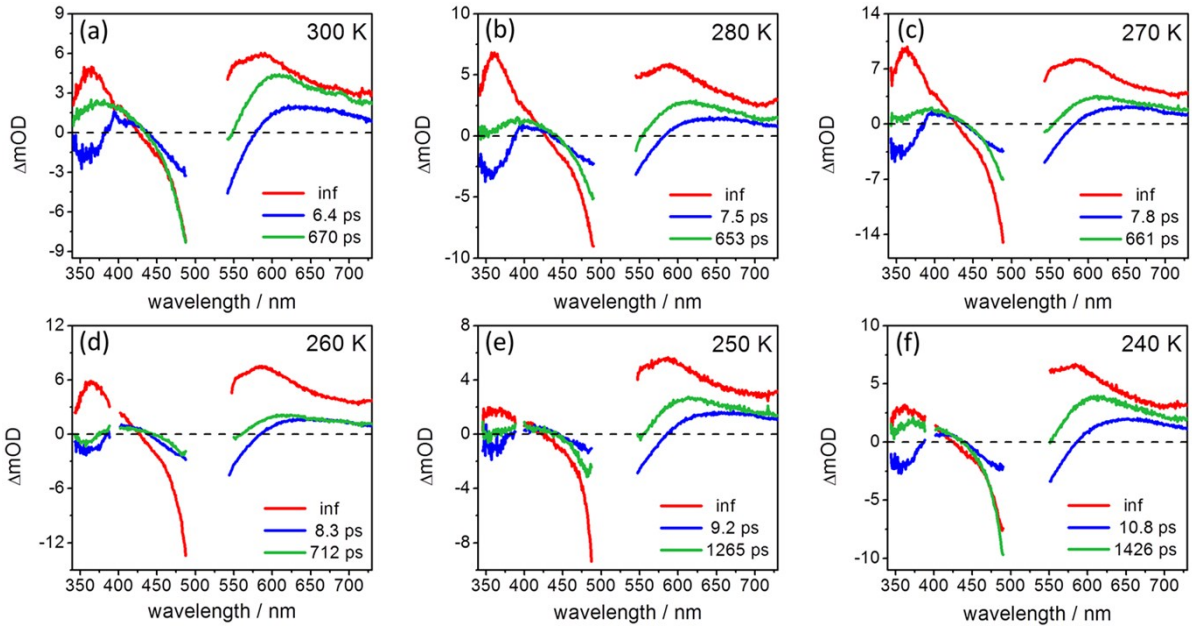


**Figure S7.** Decay-associated spectra resulting from the global fit of fs TA data upon excitation at 520 nm in dichloromethane.

Temperature dependent fs TA data of **D4**

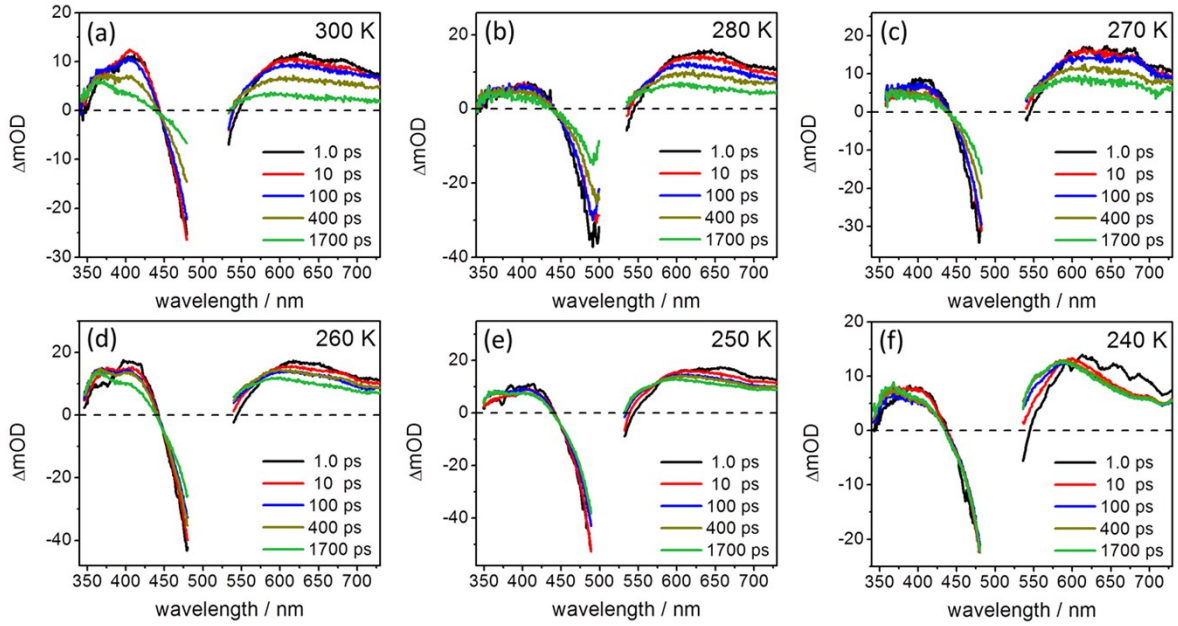


**Figure S8.** fs transient absorption spectra at selected delay times upon excitation at 520 nm in dichloromethane at temperature regions from 300 to 240 K.

It should be noted that the shape of the fs TA spectra at 240 K changes (*i.e.* 540 to 730 nm) compared to other data at higher temperatures. Meanwhile the corresponding DAS yields two kinetic components which are both faster than others (Figure S9f). The interpretation of the data at 240 K is complicated. Thus for the Marcus analysis the data point at 240 K for **D4** was omitted in the main text.

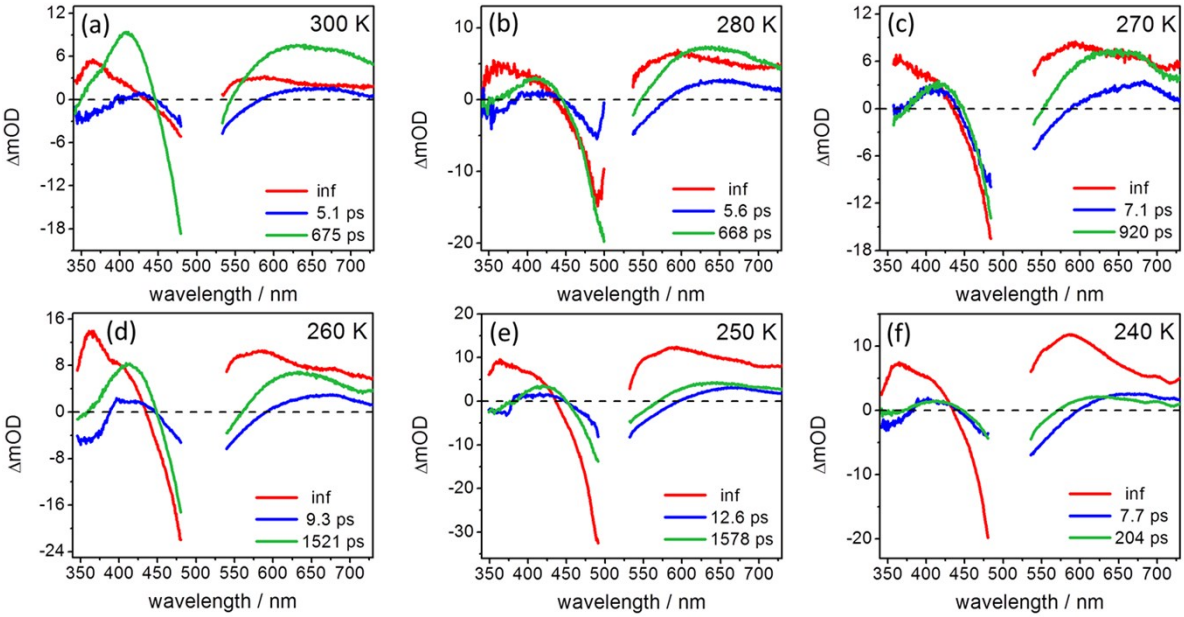


**Figure S9.** Decay-associated spectra resulting from the global fit of fs TA data upon excitation at 520 nm in dichloromethane.

Temperature dependent fs TA data of **T1**

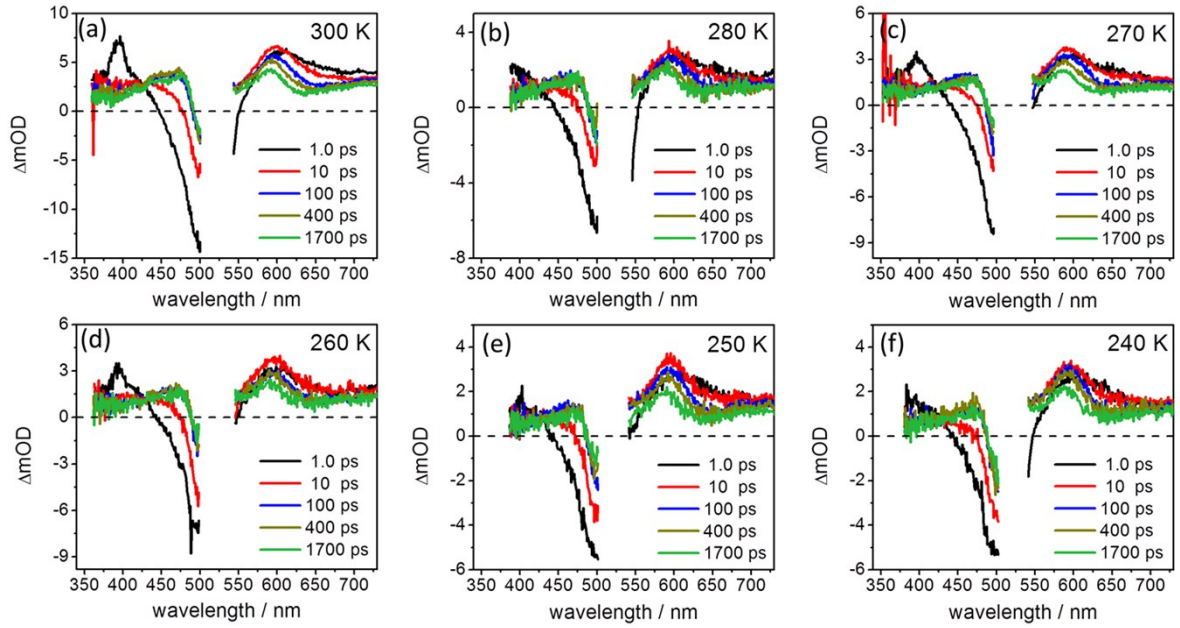


**Figure S10.** fs transient absorption spectra at selected delay times upon excitation at 520 nm in dichloromethane at temperature regions from 300 to 240 K.

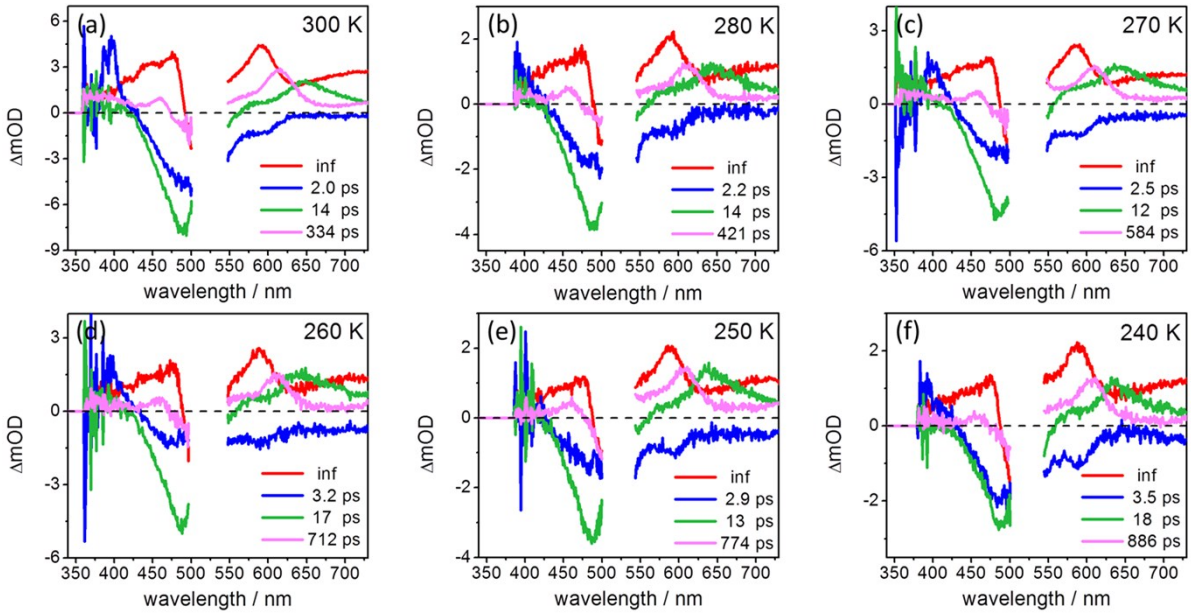


**Figure S11.** Decay-associated spectra resulting from the global fit of fs TA data upon excitation at 520 nm in dichloromethane.

Summary of the time constants for electron transfer

**Table S1.** Temperature dependence of the time constants (in ps) for the PTZ→$Ru(tpy)_2^*$ electron transfer process in **D1**–**D4** and **T1** obtained from the global fit of fs TA data.

| T / K | **D1** | **D2** | **D3** | **D4** | **T1** |
|---|---|---|---|---|---|
| 300 | 5.0 | 4.6 | 6.4 | 5.1 | 2.0 |
| 280 | 5.4 | 5.2 | 7.5 | 5.6 | 2.2 |
| 270 | 5.2 | 5.6 | 7.8 | 7.1 | 2.5 |
| 260 | 6.4 | 5.9 | 8.3 | 9.3 | 3.2 |
| 250 | 7.1 | 6.8 | 9.2 | 12.6 | 2.9 |
| 240 | 8.3 | 7.6 | 10.8 | – | 3.5 |

Estimation of reorganization energy and the temperature dependence

$$\lambda = \lambda_i + \lambda_o \quad (1)$$

$$\lambda_o = \frac{e^2}{4 \cdot \pi \cdot \varepsilon_0} \cdot \left(\frac{1}{2a_1} + \frac{1}{2a_2} - \frac{1}{R_{DA}}\right) \cdot \left(\frac{1}{n^2} - \frac{1}{\varepsilon_s}\right) \quad (2)$$

where $\lambda_i$ and $\lambda_o$ represent the inner and outer reorganization energy, respectively.[4] $\lambda_i$ reflects the free energy change associated with the nuclear bond length changes within molecules and $\lambda_o$ accounts for the reorganization of the surrounding chemical environment, *e.g.* solvent molecules. In the simplest model, electron donor and acceptor are treated as spheres with radii $a_1$ and $a_2$ (for more accurate prediction, electron donor and electron acceptor should be treated as ellipsoids).[5] $R_{DA}$ is the donor-acceptor distance. n and $\varepsilon_s$ represent refractive index and dielectric constant of the solvent involved during charge transfer, respectively. $\varepsilon_0$ is the vacuum permittivity ($8.85 \times 10^{-12}$ F/m).

For the PTZ-Ru(tpy)$_2$-R system:

1. $\lambda_i$ is estimated to be 0.1 eV[5,6] and commonly treated as distance[5] and temperature[7,8] independent.

2. Both n and $\varepsilon_s$ are temperature dependent, $\varepsilon_s(T) = a + bT + cT^2 + dT^3$, for dichloromethane, $a = 0.40452 \times 10^2$, $b = -0.17748 \times 10^0$, $c = 0.23942 \times 10^{-3}$, $d = 0$;[9]

For dichloromethane, $n(T) = 1.59078 - 5.66 \times 10^{-4}$ T.[10]

3. For PTZ→Ru(tpy)$_2^*$ electron transfer, PTZ and photo-excited Ru complex are the electron donor ($a_1$ = 4 Å) and acceptor ($a_2$ = 5 Å), respectively. The center-to-center distance $R_{DA}$ is 9.6 Å. $a_1$, $a_2$ and $R_{DA}$ were estimated from the neutral, optimized molecular structures.[2,11]

As a result, the calculated reorganization energy associated with PTZ→Ru(tpy)$_2^*$ electron transfer as a function of temperature for **D1** and **T1** were summarized in Table S3-4. Only **D1** and **T1** were exemplarily calculated since all compounds have the same electron donor, donor-acceptor distance and chemical linkage.

Estimation of driving forces and the temperature dependence

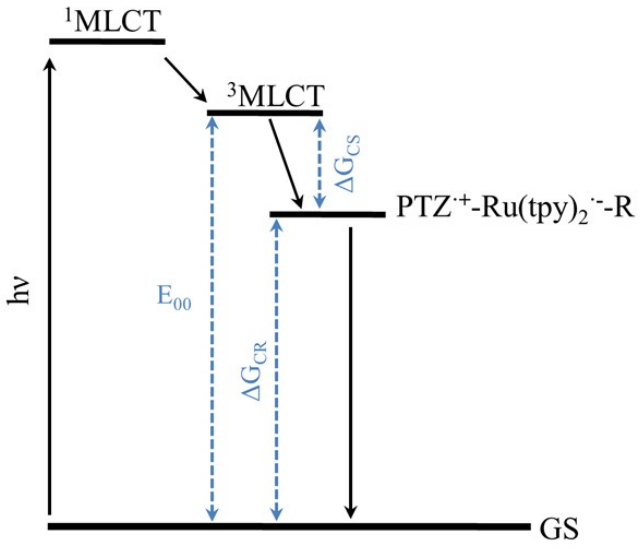


For PTZ→Ru(tpy)$_2^*$ electron transfer, the radical pairs are PTZ$^{\cdot+}$ / tpy$^{\cdot-}$. $E_{00}$ in Rehm-Weller equation is the energy difference between the excited state (where the electron transfer takes place) and ground state. In our system, as indicated in the relaxation model (see Figure S1) electron transfer occurs from an upper-lying $^3$MLCT state. Since different $^3$MLCT states are relatively close in energy, $E_{00}$ is taken to be 2.07 eV which was estimated from the emission spectrum of [Ru(tpy)$_2$](PF$_6$)$_2$ at 77 K (in butyronitrile glass).[12] The Gibbs free energy change of a photoinduced electron transfer process can be estimated by:

$$\Delta G^\circ_{CS} = e\,(E_{D^+/D} - E_{A/A^-}) - E_{00} - \frac{e^2}{4\pi\varepsilon_0\varepsilon R_{DA}} \quad (3)$$

$$\Delta G^\circ_{CR} = -\Delta G^\circ_{CS} - E_{00} \quad (4)$$

The values of $E_{PTZ+/PTZ}$ and $E_{tpy/tpy-}$ in **D1** and **T1** were taken from ref 2. For **D2-D4** cyclic voltammetry was performed (Figure S12 and Table S2). The influence of temperature on $\Delta G^\circ_{CS}$ value is also considered (see Table S3-4).

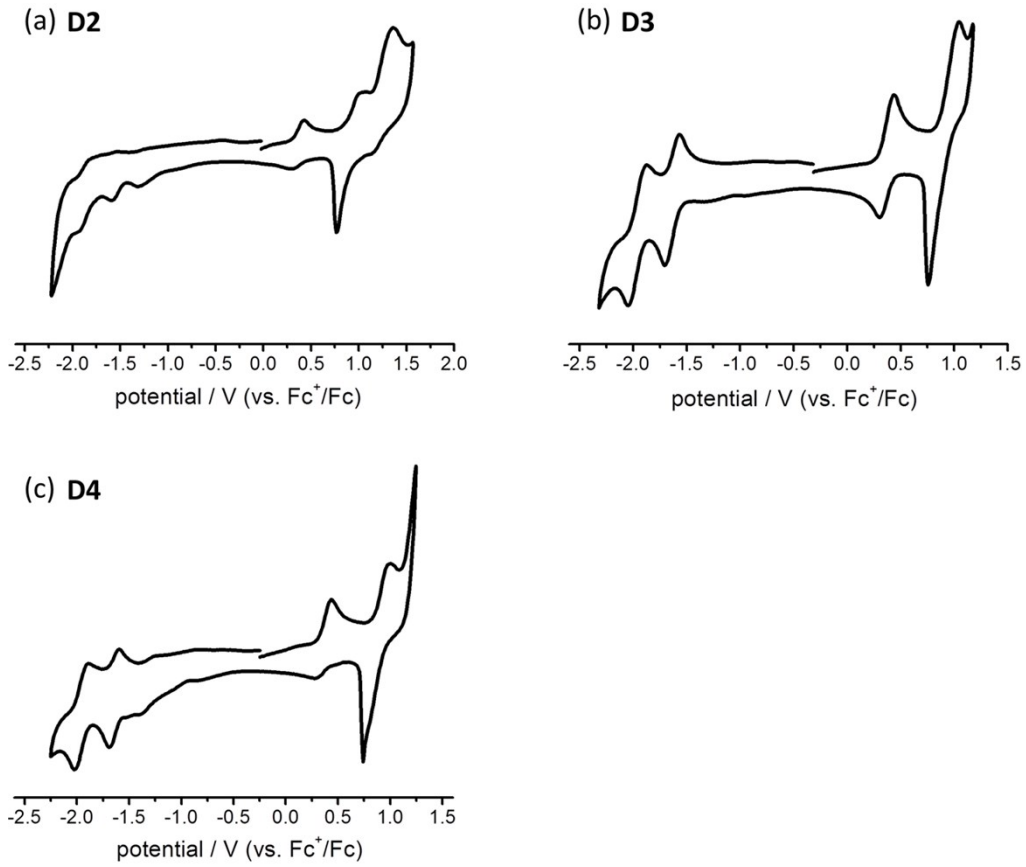


**Figure S12.** Cyclic voltammetry curves (scan rate 200 mV/s) for **D2-D4** in dichloromethane with 0.1 M $Bu_4NPF_6$ supporting electrolyte.

**Table S2.** Summary of electrochemical data for **D1-D4** and **T1** recorded in dichloromethane with 0.1 M $Bu_4NPF_6$ supporting electrolyte.

| | $E^o$ / V (vs. $Fc^{+}$/Fc) | | |
|---|---|---|---|
| | $PTZ^{+}$ / PTZ | $Ru^{III}$ / $Ru^{II}$ | tpy / $tpy^{-}$ |
| **D1**[a] | 0.35 | 0.87 | -1.60 |
| **D2** | 0.35 | 0.87 | -1.63 |
| **D3** | 0.37 | 0.90 | -1.62 |
| **D4** | 0.36 | 0.86 | -1.64 |
| **T1**[a] | 0.34 | 0.99 | -1.67 |

[a] Electrochemical data were taken from ref 2.

Summary of calculations for PTZ→Ru(tpy)$_2^*$ electron transfer

**Table S3.** Summary of the calculated temperature dependent dielectric constant (ε) and refractive index (n) of dichloromethane as well as reorganization energy (λ), driving force ($-\Delta G^\circ$) for charge separation, activation energy ($\Delta G^\ddagger$) in **D1**.

| T / K | ε | n | λ | $-\Delta G^\circ$ / eV | $\Delta G^\ddagger$ / eV[a] |
|---|---|---|---|---|---|
| 300 | 8.7558 | 1.4210 | 0.763 | 0.291 | 0.073 |
| 280 | 9.5281 | 1.4323 | 0.766 | 0.277 | 0.078 |
| 260 | 10.4920 | 1.4436 | 0.769 | 0.263 | 0.083 |
| 240 | 11.6474 | 1.4549 | 0.773 | 0.249 | 0.089 |

**Table S4.** Summary of the calculated temperature dependent dielectric constant (ε) and refractive index (n) of dichloromethane as well as reorganization energy (λ), driving force ($-\Delta G^\circ$) for charge separation, activation energy ($\Delta G^\ddagger$) in **T1**.

| T / K | ε | n | λ | $-\Delta G^\circ$ / eV | $\Delta G^\ddagger$ / eV[a] |
|---|---|---|---|---|---|
| 300 | 8.7558 | 1.4210 | 0.763 | 0.231 | 0.093 |
| 280 | 9.5281 | 1.4323 | 0.766 | 0.217 | 0.098 |
| 260 | 10.4920 | 1.4436 | 0.769 | 0.203 | 0.104 |
| 240 | 11.6474 | 1.4549 | 0.773 | 0.189 | 0.110 |

[a] Activation energy was obtained by $(\lambda+\Delta G°)^2/4\lambda$.[13,14]

The influence of temperature on solvent dielectric properties, *i.e.* dielectric constant ε and refractive index n, which may change λ (eq S1-2) and $-\Delta G^\circ$ (eq S3-4), is considered in this work. It should be noted that the single linear relation indicated by the reformed Marcus equation in the main text can really be expected when both λ and the term $(\lambda+\Delta G°)^2/4\lambda$ (*i.e.* activation energy, $\Delta G^\ddagger$) are temperature independent.[13,14] Otherwise, deviation from single linear regression would be observed because of the impact of temperature on solvent dielectric properties.[13,14] According to Table S3-4, λ and $\Delta G^\ddagger$ are apparently insensitive to temperature variation which show relative small changes of 0.010 and 0.017 eV, respectively. Hence, we conclude that the solvent itself would not cause significant deviations due to temperature change.

Molecular structure of the reference compounds

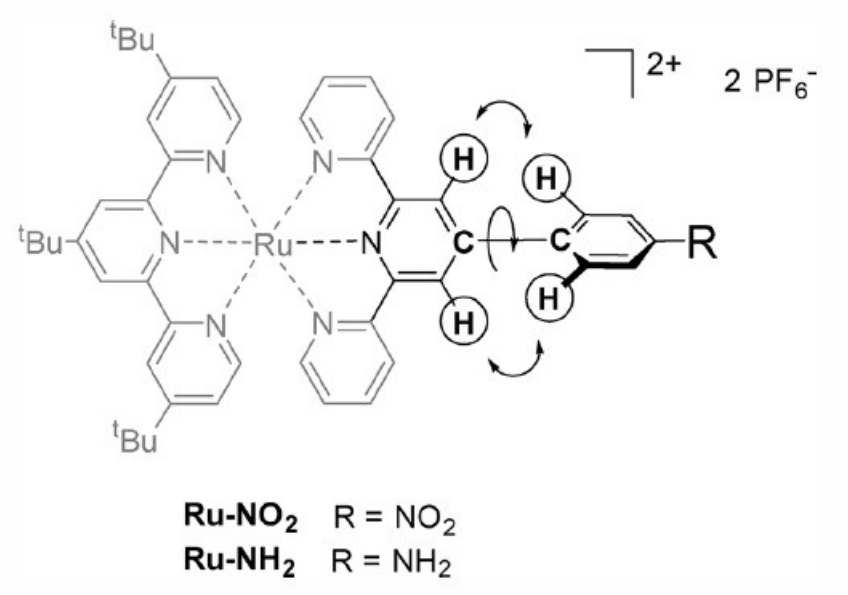


**Figure S13.** Molecular structure of the functionalized $Ru(tpy)_2$ complexes with a strongly electron donating substituent $–NH_2$ and a strongly electron withdrawing substituent $–NO_2$ referred in the main text.[15,16]

NMR spectra of **D2**

*$^{1}H$ NMR (400 MHz, $CD_3CN$)*

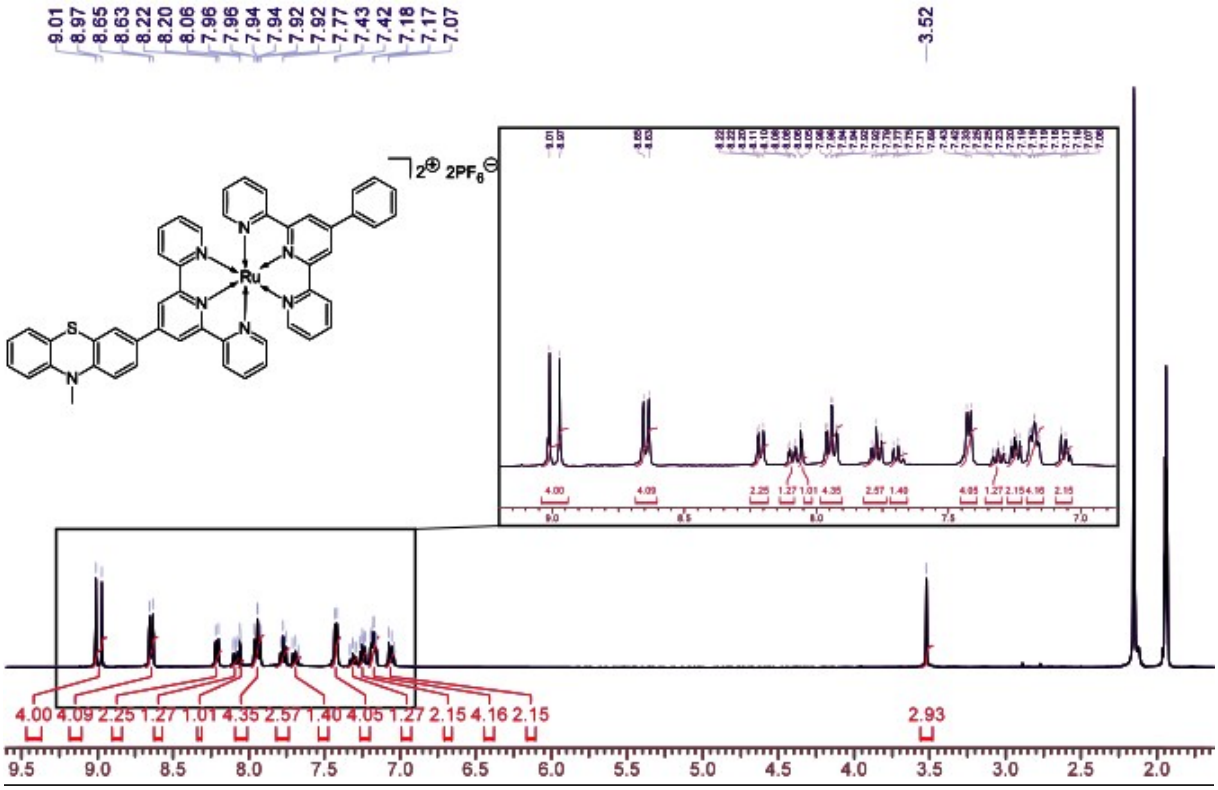


*$^{13}C$ NMR (101 MHz, $CD_3CN$)*

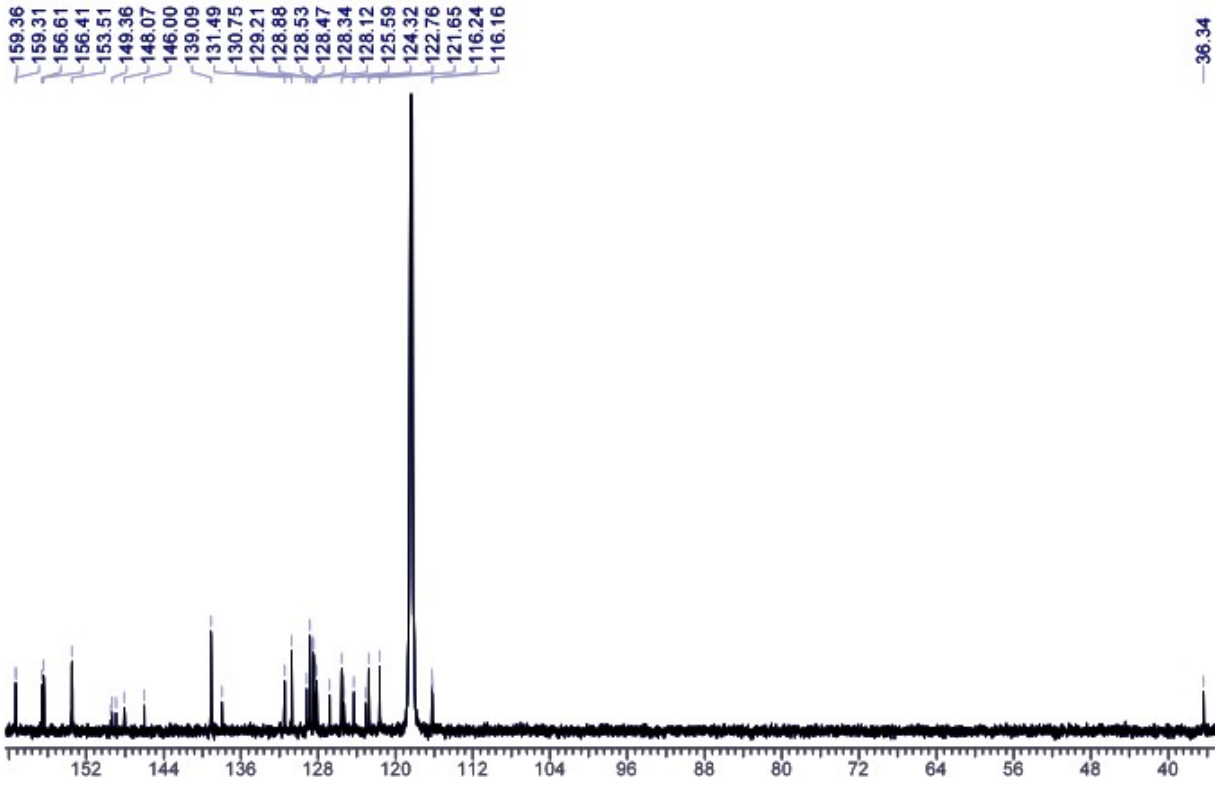

NMR spectra of **D3**

*$^{1}$H NMR (400 MHz, $CD_3CN$)*

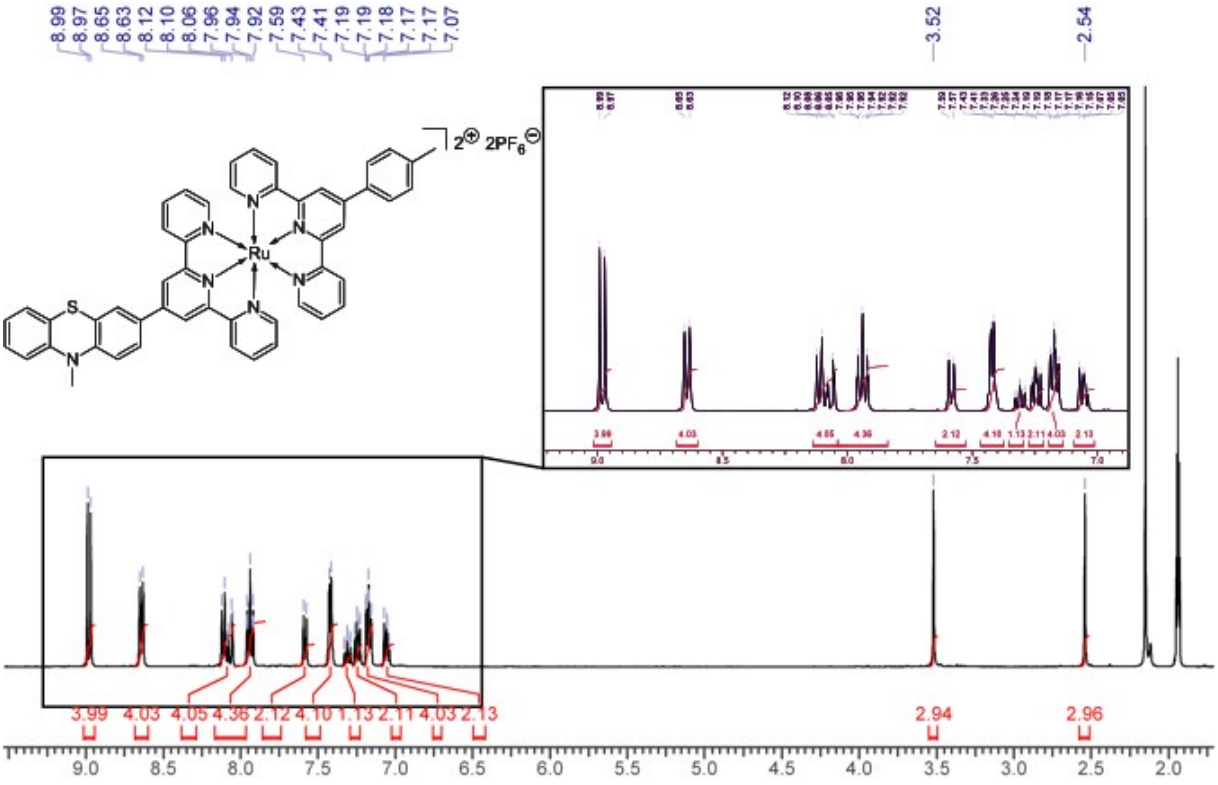


*$^{13}$C NMR (101 MHz, $CD_3CN$)*

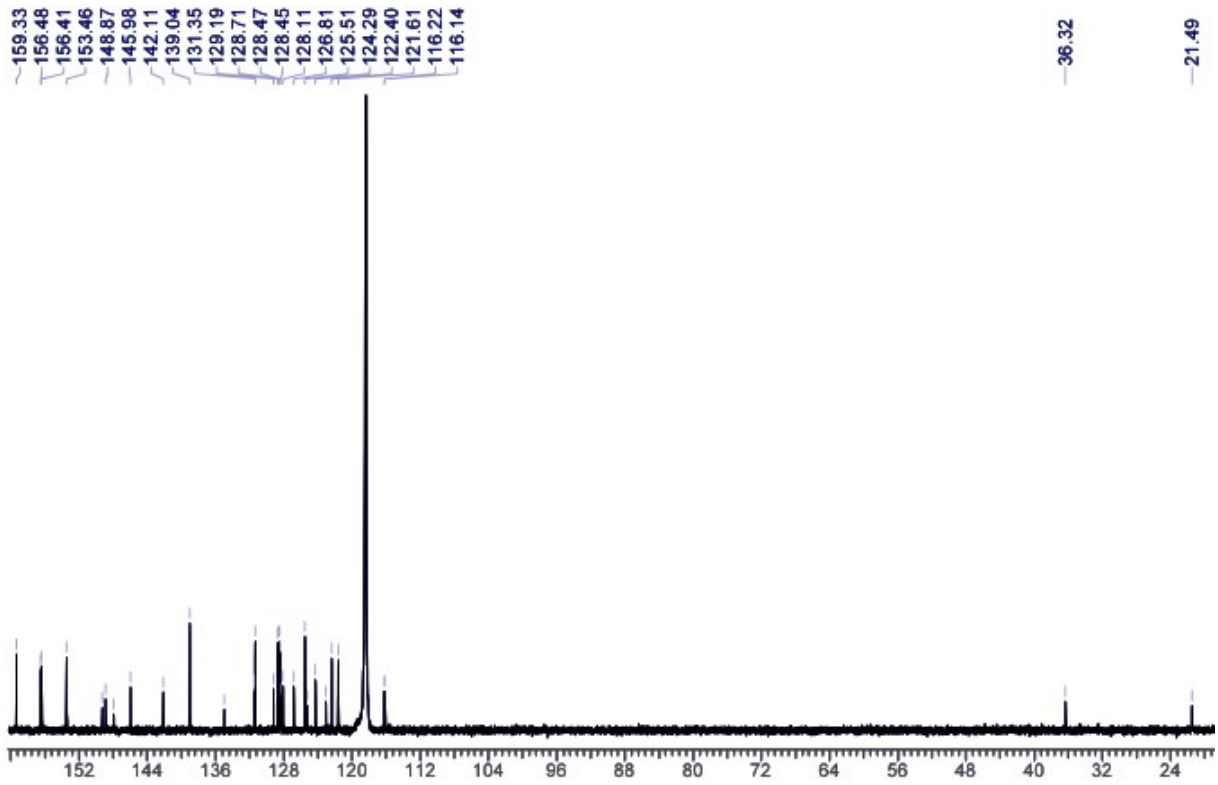

NMR spectra of **D4**

*$^{1}$H NMR (400 MHz, $CD_3CN$)*

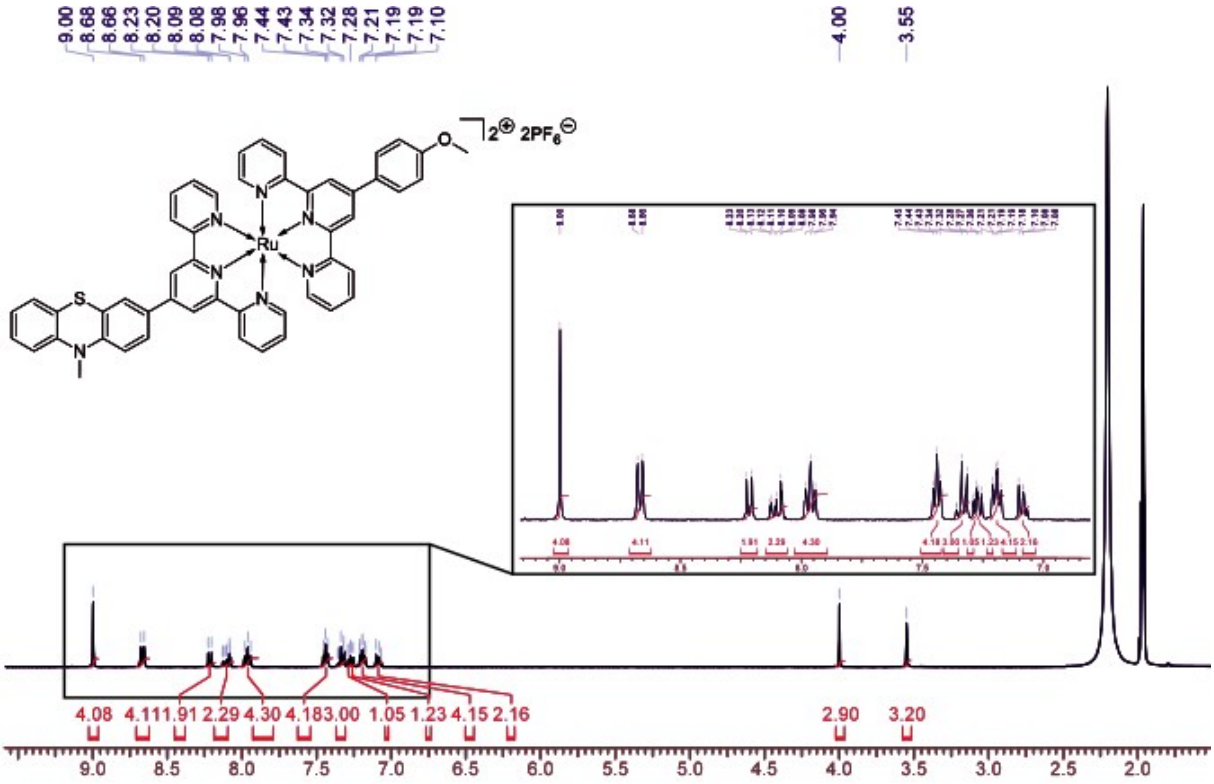


*$^{13}$C NMR (101 MHz, $CD_3CN$)*

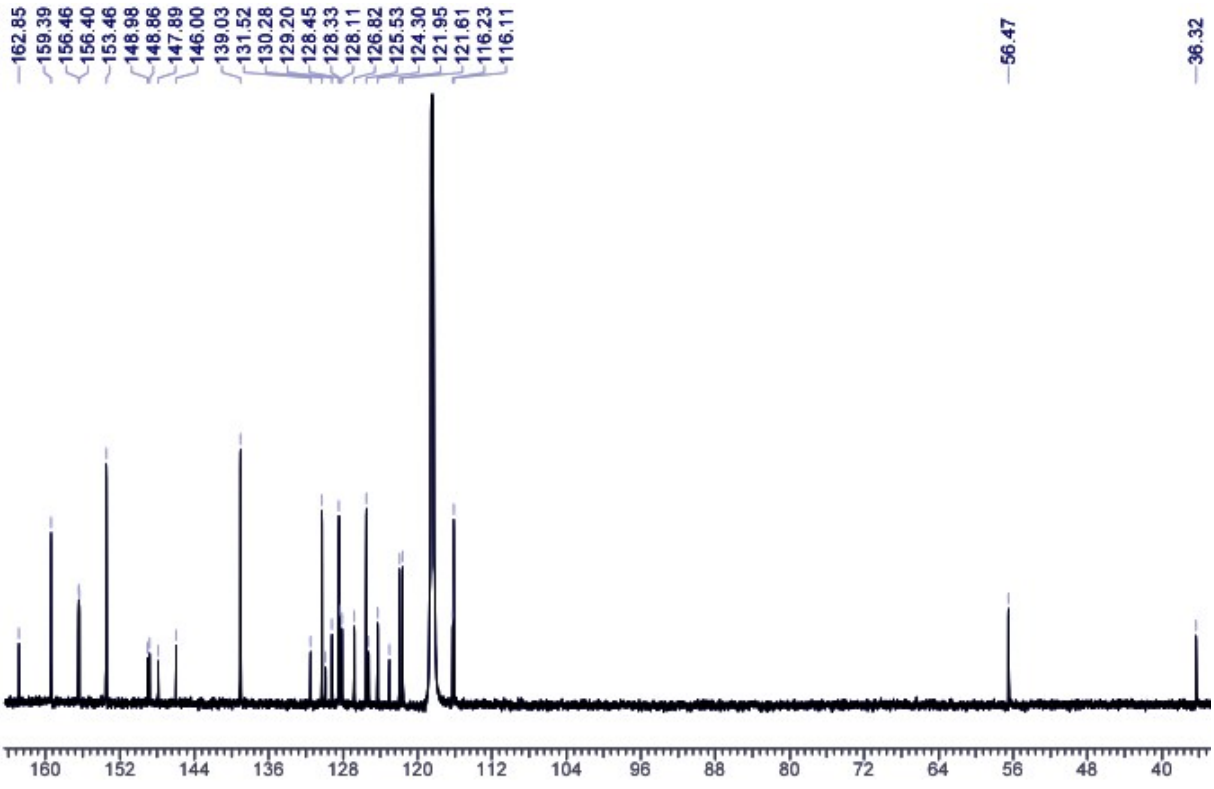

## REFERENCES


1. K. Barthelmes, J. Kübel, A. Winter, M. Wächtler, C. Friebe, B. Dietzek and U. S. Schubert, *Inorg. Chem.*, 2015, **54**, 3159−3171.

2. K. Barthelmes, A. Winter and U. S. Schubert, *Eur. J. Inorg. Chem.*, 2016, **2016**, 5132–5142.

3. Y. Luo, K. Barthelmes, M. Wächtler, A. Winter, U. S. Schubert and B. Dietzek, *Chem. Eur. J.*, 2017, **23**, 4917–4922.

4. R. A. Marcus and N. Sutin, *Biochim. Biophys. Acta*, 1985, **811**, 265–322.

5. M. Kuss-Petermann and O. S. Wenger, *Phys. Chem. Chem. Phys.*, 2016, **18**, 18657–18664.

6. E. Göransson, J. Boixel, J. Fortage, D. Jacquemin, H.-C. Becker, E. Blart, L. Hammarström and F. Odobel, *Inorg. Chem.*, 2012, **51**, 11500−11512.

7. J. Kroon, H. Oevering, J. W. Verhoeven, J. M. Warman, A. M. Oliver and M. N. Paddon-Row, *J. Phys. Chem.*, 1993, **97**, 5065–5069.

8. P. Vath, M. B. Zimmt, D. V. Matyushov and G. A. Voth, *J. Phys. Chem. B*, 1999, **103**, 9130–9140.

9. D. R. Lide, *Handbook of Chemistry and Physics*, 84$^{th}$ edition.

10. H. Shekaari, A. Bezaatpour and A. Soltanpour, *J. Chem. Eng. Data*, 2010, **55**, 5927–5931.

11. Y. Luo, K. Barthelmes, M. Wächtler, A. Winter, U. S. Schubert and B. Dietzek, *J. Phys. Chem. C*, 2017, **121**, 9220–9229.

12. J.-P. Sauvage, J.-P. Collin, J.-C. Chambron, S. Guillerez, C. Coudret, V. Baltani, F. Barigelletti, L. D. Cola and L. Flamigni, *Chem. Rev.*, 1994, **94**, 993–1019.

13. J. Kroon, H. Oevering, J. W. Verhoeven, J. M. Warman, A. M. Oliver and M. N. Paddon-Row, *J. Phys. Chem.*, 1993, **97**, 5065–5069.

14. R. H. Goldsmith, O. DeLeon, T. M. Wilson, D. Finkelstein-Shapiro, M. A. Ratner and M. R. Wasielewski, *J. Phys. Chem. A*, 2008, **112**, 4410–4414.

15. M. Presselt, B. Dietzek, M. Schmitt, S. Rau, A. Winter, M. Jäger, U. S. Schubert and J. Popp, *J. Phys. Chem. A*, 2010, **114**, 13163–13174.

16. J. Preiß, M. Jäger, S. Rau, B. Dietzek, J. Popp, T. Martínez and M. Presselt, *ChemPhysChem*, 2015, **16**, 1395–1404.